# The Combined Influence of Observed Southern Ocean Clouds and Sea Ice on Top-of-Atmosphere Albedo

W. R. Frey, A. L. Morrison, J. E. Kay, R. Guzman, H. Chepfer

Journal of Geophysical Research: Atmospheres

RESEARCH ARTICLE
10.1029/2018JD028505

# The Combined Influence of Observed Southern Ocean Clouds and Sea Ice on Top-of-Atmosphere Albedo

W. R. Frey[1,2], A. L. Morrison[1,2], J. E. Kay[1,2], R. Guzman[3], and H. Chepfer[4]

[1]Cooperative Institute for Research in Environmental Sciences, University of Colorado Boulder, Boulder, CO, USA, [2]Atmospheric and Oceanic Sciences, University of Colorado Boulder, Boulder, CO, USA, [3]LMD/IPSL, CNRS, Ecole Polytechnique, Palaiseau, France, [4]Sorbonne Université, École polytechnique, École normale supérieure, PSL Research University, CNRS, Paris, France

**Key Points:**
- Southern Ocean low cloud cover is unchanged in summer and slightly higher in spring over open water compared to sea ice
- In spring and summer, Southern Ocean cloud opacity increases over open water compared to sea ice
- Despite the cloud response, top-of-atmosphere albedo is lower and more shortwave radiation is absorbed over open water than over sea ice

**Correspondence to:**
W. R. Frey,
william.frey@colorado.edu

**Citation:**
Frey, W. R., Morrison, A. L., Kay, J. E., Guzman, R., & Chepfer, H. (2018). The combined influence of observed Southern Ocean clouds and sea ice on top-of-atmosphere albedo. *Journal of Geophysical Research: Atmospheres*, *123*, 4461–4475. https://doi.org/10.1029/2018JD028505

Received 8 FEB 2018
Accepted 8 APR 2018
Accepted article online 16 APR 2018
Published online 8 MAY 2018



**Abstract** When sea ice concentration decreases, surface albedo decreases. Yet the impact of Southern Ocean sea ice concentration decreases on top-of-atmosphere albedo is uncertain. Why? The cloud cover and opacity response to Southern Ocean sea ice variability has been challenging to quantify. Here we use observations to constrain the cloud response to Southern Ocean sea ice variability and assess the combined influence of sea ice and clouds on top-of-atmosphere albedo. We focus on the spring and summer seasons that dominate the high-latitude shortwave energy budget. To isolate the influence of sea ice concentration on clouds, we analyze spaceborne light detection and ranging (LIDAR) observations in regions where present-day sea ice concentration varies. During spring, low cloud cover is slightly (4%) higher over open water compared to sea ice. During summer, sea ice variability does not affect low cloud cover. During both spring and summer, cloud opacity is larger over open water than over sea ice due to a cloud phase shift from ice toward liquid with warming. Independent ship-based visual and radiosonde observations available during summer corroborate the LIDAR results. Even with the cloud response, satellite-observed top-of-atmosphere albedo is lower over open water than over sea ice. The observations show the cloud response to sea ice retreat with warming will not mask the surface albedo decrease. In other words, more shortwave radiation will be absorbed when Southern Ocean sea ice is lost.

## 1. Introduction

Both clouds and sea ice influence Earth's energy budget by reflecting incoming shortwave radiation back to space. Sea ice has a strong influence on surface albedo, as sea ice is much more reflective than open ocean. Changes in surface albedo account for more than half of the interannual variability in planetary albedo (Qu & Hall, 2005). As the climate warms, sea ice is expected to retreat exposing more open ocean and decreasing surface albedo. However, cloud changes occurring in the same region as sea ice changes also influence top-of-atmosphere albedo (e.g., Hartmann & Ceppi, 2014). If the cloud response to sea ice retreat cannot completely compensate for the surface albedo decrease, top-of-atmosphere albedo will decrease. As a result, more shortwave radiation will be absorbed and accelerate warming (Fitzpatrick & Warren, 2007; Morrison et al., 2018; Qu & Hall, 2005).

Sea ice interacts with clouds at both poles. Yet the Arctic and the Southern Ocean sea ice zone (poleward of 60°S) differ in important ways. The Southern Ocean sea ice zone is confined to equatorward of ~70°S due to the presence of Antarctica. In contrast, the Arctic Ocean and Arctic sea ice zone cover the North Pole. When compared to the Arctic, Southern Ocean sea ice-cloud interactions are more strongly influenced by deep ocean circulation (Marshall & Speer, 2012) and an all-season midlatitude storm track. Recent trends in Arctic and Southern Ocean sea ice extent are opposite, with decreased Arctic sea ice extent and increased Southern Ocean sea ice extent (Simmons, 2015; Stammerjohn et al., 2012). Finally, each hemisphere is expected to respond to climate change differently, with the Arctic warming faster than the global average (Serreze et al., 2009), while the Southern Ocean warms more slowly than the global average (Armour et al., 2016). Given these differences, the relationship between sea ice and clouds in the Arctic and over the Southern Ocean must be assessed separately.

In the Arctic, the impact of sea ice on clouds has been quantified and the underlying physical mechanisms have been identified (see review paper by Kay et al., 2016). During spring and fall, cloud cover and optical depth are larger over open water compared to over sea ice (Eastman & Warren, 2010; Kay & Gettelman,

2009; Morrison et al., 2018; Palm et al., 2010; Schweiger et al., 2008). During summer, there is no significant difference in either cloud cover or optical depth over open water compared with sea ice (Kay & Gettelman, 2009; Kay & L'Ecuyer, 2013; Morrison et al., 2018). The relationship between clouds and Arctic sea ice may depend on atmospheric conditions (e.g., stability and subsidence) that influence air-sea coupling (Barton et al., 2012; Taylor et al., 2015). In fact, the seasonal difference in cloud response to sea ice is due to the strength of air-sea coupling that is weaker during summer than other seasons (Morrison et al., 2018).

Over the Southern Ocean, the impact of sea ice on clouds is known during Austral winter but less certain during Austral spring and summer. In winter, sea ice and clouds are strongly linked, with low cloud cover increasing by 20–30% over open water compared to sea ice (Wall, Kohyama, et al., 2017). Similarly, annual mean cloud cover is greater over open water than over sea ice (Bromwich et al., 2012). During spring and summer, relatively sparse ship-based observations of clouds and solar irradiance suggest that clouds are more prevalent and optically thicker over open water than over sea ice, though this finding could be influenced by latitudinal variation (Fitzpatrick & Warren, 2007). The impact of Southern Ocean sea ice variability on top-of-atmosphere albedo, which determines how much shortwave radiation is absorbed, depends strongly on the cloud response. If clouds remain unchanged as sea ice retreats more shortwave radiation is absorbed, but if cloud cover or opacity increase as sea ice retreats the amount of absorbed shortwave radiation may decrease (Fitzpatrick & Warren, 2007).

Building on previous work, the goal of this study is to constrain the cloud and top-of-atmosphere albedo response to Southern Ocean sea ice variability. We focus on Austral spring and summer that dominate the Southern Ocean shortwave energy budget (e.g., Fitzpatrick & Warren, 2007). The Southern Ocean shortwave energy budget is particularly important because the Southern Ocean, including the sea ice zone poleward of 60°S, is one of the only regions of the globe where models robustly predict a negative shortwave cloud radiative feedback (Zelinka et al., 2012). The magnitude of this negative feedback has a large impact on climate sensitivity (Frey et al., 2017; Frey & Kay, 2018; Tan et al., 2016) and could be influenced by sea ice-cloud interactions.

Historically, research on Southern Ocean sea ice-cloud interactions has been limited by a lack of reliable observations. Reanalysis products contain large errors over the Southern Ocean due to the lack of observational constraints (Bromwich et al., 2007; Bromwich & Fogt, 2004; Bromwich et al., 2011; Hines et al., 1999; Jones et al., 2016; Marshall, 2002; Nicolas & Bromwich, 2011). Additionally, reliable cloud observations are limited because they must be independent of surface condition to identify the impact of sea ice on clouds. Passive satellite observations of clouds (e.g., from the Moderate Resolution Imaging Spectrometer, MODIS) are not independent of surface condition (Kay & L'Ecuyer, 2013; Liu et al., 2010). Using reanalysis and passive satellite observations to identify sea ice-cloud interactions can produce results different from those arrived at with surface-independent observations (Eastman & Warren, 2010; Kay & Gettelman, 2009; Morrison et al., 2018; Palm et al., 2010).

With this study, we overcome the limitations of previous studies by using two independent observational data sets that are both independent of surface conditions: (1) spaceborne light detection and ranging (LIDAR) and (2) visual ship-based observations. Following Morrison et al. (2018), we restrict our analysis to areas where sea ice concentration varies. Thus, we ensure that our findings are not an artifact of geographic (latitudinal) variations in cloud properties. We find similar cloud changes using the independent satellite and surface-based data sets. The observations we analyze suggest that the cloud response to sea ice variability is not enough to compensate for the change in surface albedo. In other words, even when the cloud response is included, top-of-atmosphere albedo is lower and more shortwave radiation is absorbed over open water compared to over sea ice.

## 2. Data and Methods

### 2.1. Data

To isolate the relationship between sea ice and clouds, we use observations that are independent of the underlying surface condition and available at daily or higher time frequency. We primarily use a decade (2006–2015) of observations from the Cloud-Aerosol LIDAR with Orthogonal Polarization (CALIOP) instrument (Winker et al., 2007) onboard the Cloud-Aerosol Lidar and Infrared Pathfinder Satellite Observation

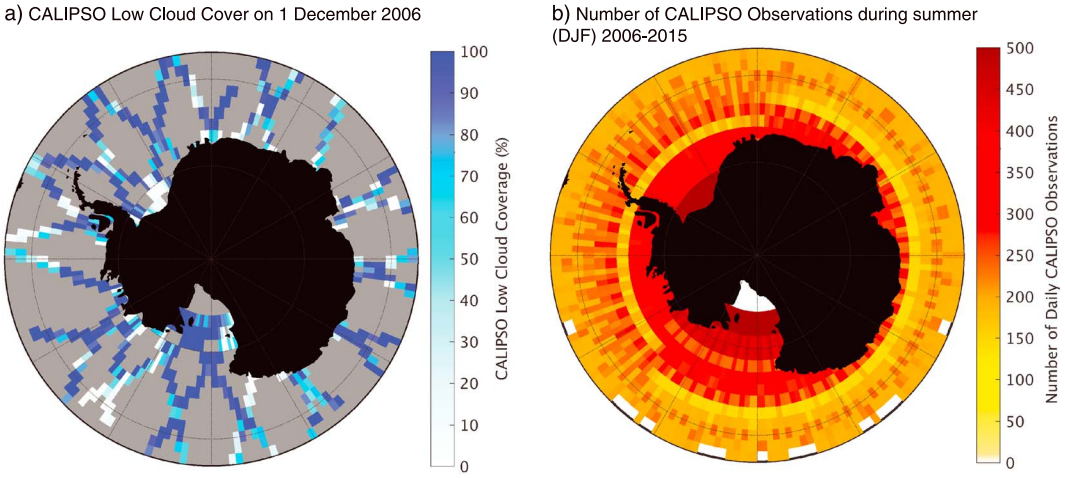


**Figure 1.** CALIPSO-GOCCP data demonstration. (a) A single day (1 December 2006) of CALIPSO low cloud cover data on the 2 × 2° GOCCP output grid (Chepfer et al., 2010). (b) Number of daily CALIPSO low cloud cover observations in each grid cell for summer (December, January, and February [DJF]) during our study period (2006–2015). Gray area in (a) shows grid cells with no CALIPSO data on 1 December 2006.

(CALIPSO) satellite. As an active sensor, CALIPSO cloud observations are not influenced by surface conditions. Our cloud cover analysis is based on the CALIPSO General Circulation Model-Oriented CALIPSO Cloud Product (CALIPSO-GOCCP) version 2.9 (Chepfer et al., 2010). CALIPSO-GOCCP provides daily cloud cover on a 2 × 2° grid with a 480-m vertical resolution. Cloud cover is provided at low (Pressure > 680 hPa), middle (680 > Pressure > 440 hPa), and high (Pressure < 440 hPa) levels as well as total cloud cover. Clouds are detected for individual profiles taken every 333 m along track in the CALIPSO footprint (70-m diameter) (Winker et al., 2007). Cloud cover is defined for each grid cell and day as the number of cloudy profiles divided by the total number of profiles. CALIPSO data for any given day is relatively sparse, and daily cloud cover in a grid cell is defined by a single satellite pass. Using daily data from a 10-year period provides full spatial coverage over the Southern Ocean with multiple days of observations in each grid cell (Figure 1). In addition, our 10-year sample minimizes biases linked to the small CALIPSO footprint (Konsta et al., 2016) and allows us to identify relationships between clouds and sea ice.

To analyze cloud optical depth, we use daytime opaque and thin cloud cover from CALIPSO-GOCCP version 3.0 (Guzman et al., 2017). The opaque/thin product classifies clouds based on LIDAR attenuation. Clouds that fully attenuate the LIDAR (optical depth >~3, no surface echo detected) are classified as opaque, while scenes where the LIDAR is not fully attenuated (optical depth <3, surface echo detected) are classified as thin. This definition of thin clouds includes both scenes that are covered with clouds with optical depth <3 and scenes where the CALIPSO footprint (70-m diameter) is partially filled with cloud such that the LIDAR is not fully attenuated even though the clouds that exist in the footprint may individually be optically thick (Leahy et al., 2012). We use these definitions to define opaque cloud fraction, or the opaque cloud cover divided by the total (opaque plus thin) cloud cover. The altitude of LIDAR attenuation is also provided. While the opaque/thin product is limited in that it only provides information on whether cloud optical depth is greater or less than ~3, it is a direct measurement that is not influenced by surface condition. Cloud shortwave radiative properties change near an optical depth of 3 and continue to change with increasing optical depth (Zelinka et al., 2012, Figure 1b). Therefore, the CALIPSO attenuation threshold does provide meaningful, if not complete, information about a cloud's impact on top-of-atmosphere albedo.

We pair CALIPSO cloud observations with coincident satellite-based observations of sea ice concentration and top-of-atmosphere albedo. Daily sea ice observations are from the National Snow and Ice Data Center (NSIDC) Climate Data Record of Passive Microwave Sea Ice Concentration, version 3 (Meier et al., 2017; Peng et al., 2013). NSIDC sea ice data are published on a 25 × 25-km polar-stereographic grid, and we regridded to a 2 × 2° grid to match CALIPSO-GOCCP. To assess the combined influence of sea ice and cloud changes on top-of-atmosphere albedo and absorbed shortwave radiation, we use the Clouds and Earth's Radiant Energy System (CERES) Single Scanner Footprint 1° (SSF1deg) data set (Loeb et al., 2005), which

**Table 1**
*Summer Cruises of the Icebreaker Polarstern Used in This Study*

| Cruise label | Start date (dd-mm-yy) | End date (dd-mm-yy) | Location | Surface meteorological observations DOI | Meteorological soundings DOI |
|---|---|---|---|---|---|
| ANT-XX/2 | 24-11-02 | 23-01-03 | Weddell Sea | 10.1594/PANGAEA.269520 | 10.1594/PANGAEA.849363 |
| ANT-XXI/2 | 17-11-03 | 19-01-04 | Weddell Sea | 10.1594/PANGAEA.269515 | 10.1594/PANGAEA.849352 |
| ANT-XXII/2 | 5-11-04 | 19-01-05 | Weddell Sea | 10.1594/PANGAEA.267682 | 10.1594/PANGAEA.849228 |
| ANT-XXIII/2 | 1811-05 | 13-01-06 | Lazarev Sea | 10.1594/PANGAEA.544827 | 10.1594/PANGAEA.849142 |
| ANT-XXIII/8 | 23-11-06 | 30-01-07 | Weddell Sea | 10.1594/PANGAEA.692881 | 10.1594/PANGAEA.849135 |
| ANT-XXIV/2 | 28-11-07 | 04-02-08 | Weddell Sea | 10.1594/PANGAEA.692890 | 10.1594/PANGAEA.845087 |
| ANT-XXV/2 | 05-12-08 | 05-01-09 | Lazarev Sea | 10.1594/PANGAEA.716896 | 10.1594/PANGAEA.845089 |
| ANT-XXVI/2 | 27-11-09 | 26-01-10 | South Pacific | 10.1594/PANGAEA.743579 | 10.1594/PANGAEA.849053 |
| ANT-XXVII/2 | 28-11-10 | 05-02-11 | South Atlantic | 10.1594/PANGAEA.760392 | 10.1594/PANGAEA.849045 |
| ANT-XXVIII/2 | 03-12-11 | 05-01-12 | South Atlantic | 10.1594/PANGAEA.784458 | 10.1594/PANGAEA.844866 |
| ANT-XXIX/2 | 30-11-12 | 18-01-13 | South Atlantic | 10.1594/PANGAEA.815476 | 10.1594/PANGAEA.844856 |
| ANT-XXIX/9 | 19-412-13 | 05-03-14 | Weddell Sea | 10.1594/PANGAEA.832606 | 10.1594/PANGAEA.844805 |
| ANT-XXXI/2 | 06-12-15 | 1402-16 | Weddell Sea | 10.1594/PANGAEA.861438 | 10.1594/PANGAEA.861658 |

*Note*. While cruises include nonsummer months, only data from summer months (December, January, and February) were used. During each cruise, visual observations of sea ice and cloud cover were taken every 3 hr (König-Langlo et al., 2006) and meteorological soundings were launched daily near 10 UTC (Driemel et al., 2016). DOI = Digital Object Identifier.

provides daily observed all-sky top-of-atmosphere flux values from CERES along with solar insolation from Solar Radiation and Climate Experiment (SORCE) Total Solar Irradiance (TSI) (Kopp et al., 2005) on a $1 \times 1°$ latitude-longitude grid.

The satellite data sets outlined above provide extensive spatial and temporal cover but also have limitations. Notably, CALIPSO LIDAR observations provide no information about clouds below the altitude of attenuation, which occurs near an optical depth of 3 (Chepfer et al., 2010). Ship-based observations provide an independent observation of clouds to compare to CALIPSO. We use ship-based visual sea ice and low cloud cover observations (König-Langlo et al., 2006) along with soundings of temperature, pressure, and relative humidity (Driemel et al., 2016) taken during 13 cruises during Austral summer between 2002 and 2016 (Table 1). We limit our use of visual cloud observations to low cloud cover observations taken during daylight hours, the type of visual cloud observations shown to be most accurate (Town et al., 2007; Warren et al., 2007).

### 2.2. Methods

Two methods are used to analyze how clouds respond to sea ice variability. In the first method, we follow Wall, Kohyama, et al. (2017). We composite low cloud cover based on meridional distance from the sea ice edge. Using daily data without interpolation, we define the sea ice edge for each longitude and day as the furthest equatorward grid cell with sea ice concentration $\geq$35%. We then bin cloud cover data poleward and equatorward of the sea ice edge (±6° latitude). This process is repeated for each day and each longitude before results are averaged to produce mean low cloud cover as a function of meridional distance from the sea ice edge. As discussed below, this method could be influenced by latitudinal variations in clouds unrelated to sea.

In the second method, we follow Morrison et al. (2018). We focus on the grid cell level and limit our analysis to areas where sea ice concentration changes. Unlike the first method, this second method removes the impact of latitudinal variations in cloud properties and isolates the cloud response to sea ice variability. Similar to Morrison et al. (2018) for the Arctic, we define an intermittent surface mask for the Southern Ocean. For each season, we consider the daily sea ice concentration over our 10-year sample (2006–2015) in a given grid cell and whether or not we have satellite cloud observations for that grid cell on a given day. A grid cell is included in the intermittent mask if both of the following conditions are met: (1) There are at least 10 days where the grid cell has sea ice concentration $<$ 15% (defined as Open Water) and we have satellite observations in the grid cell and (2) there are at least 10 days where the grid cell has sea ice concentration $>$ 80% (defined as Sea Ice) and we have satellite observations in the grid cell. All grid cells that do not meet both criteria are excluded from the intermittent mask.

With the intermittent mask defined, we use it to diagnose how clouds respond to sea ice variability. To diagnose the low cloud cover response to sea ice variability, we compare mean low cloud cover within the intermittent mask on days with open water with mean low cloud cover within the intermittent mask on

days with sea ice. A similar comparison is done for opaque cloud fraction and top-of atmosphere albedo. Because our intermittent mask depends on both sea ice concentration and the availability of satellite data, it is slightly different for each satellite data set (CALIPSO low cloud cover, CALIPSO opaque cloud fraction, and CERES top-of-atmosphere albedo) we consider. The diagnosed cloud response to sea ice variability does not depend on our choice to use 10 days as the requirement for sea ice and open water days within the intermittent mask. Different choices (i.e., 1 or 50 days) produce similar results with the primary impact being a change in size of the intermittent mask.

## 3. Results

### 3.1. Seasonal Sea Ice Concentration and Low Cloud Cover

We begin by assessing seasonal sea ice concentration and low cloud cover over the high-latitude Southern Ocean (poleward of 50°S). Sea ice varies seasonally (Figures 2a–2d) with concentration above 80% extending from Antarctica to near 60°S during winter (June, July, and August [JJA]) and spring (September, October, and November [SON]). During summer (December, January, February [DJF]) and fall (March, April, and May [MAM]) large sea ice concentrations are confined to the Ross and Weddell seas. The sea ice edge (defined as the furthest equatorward grid cell with sea ice concentration $\geq$35%; Wall, Kohyama, et al., 2017) exhibits considerable variability, especially in summer in the western hemisphere.

Low cloud cover also varies seasonally over the high-latitude Southern Ocean (Figures 2e–2h). Low cloud cover is highest in summer and lowest in winter. The relationship between clouds and sea ice also differs by season. In winter and fall, there is an apparent increase in low cloud cover with decreasing sea ice concentration (as in Wall, Kohyama, et al., 2017). During spring and summer, low cloud cover does not appear as closely related to sea ice concentration.

### 3.2. Spring and Summer Low Cloud Cover Across the Sea Ice Edge

One way to identify the relationship between sea ice and clouds is to composite cloud cover based on distance from the sea ice edge, as in Wall, Kohyama, et al. (2017) (first method in section 2.2). With this method, there is an apparent increase in low cloud cover equatorward of the sea ice edge compared with poleward of the sea ice edge during both spring and summer (Figure 3). We hypothesize that compositing data across the sea ice edge may be influenced by latitudinal variations in cloud cover unrelated to sea ice. In Figure 3, moving from sea ice to open water always means moving from south to north. Low cloud cover also varies in this direction (increasing from south to north near Antarctica) in ways that may be unrelated to sea ice (Figure 2). For example, latitudinal variations in low cloud cover are caused by the Southern Hemisphere storm track (e.g., Hoskins & Hodges, 2005) and patterns of vertical velocity, stability and sea surface temperatures (Wall, Hartmann, et al., 2017) that are unrelated to sea ice.

### 3.3. Spring and Summer Low Cloud Cover Response to Sea Ice Variability

A second way to identify the relationship between sea ice and clouds is by using our intermittent mask (second method in section 2.2). Within the intermittent mask during summer (Figures 4a–4c) there is no significant change in low cloud cover over open water compared with sea ice. During spring (Figures 4d–4f) there is a small (4.5%) increase in low cloud cover over open water compared to sea ice. During both seasons, the impact of sea ice on low cloud cover appears smaller when the intermittent mask is used compared with compositing data across the sea ice edge (Figure 3). We trust the intermittent mask result (Figure 4) because it more clearly reflects the low cloud cover response to sea ice variability independent of latitudinal variations of cloud properties. Yet the intermittent mask is limited by use of LIDAR data that provides no information about clouds occurring below the altitude of attenuation (Chepfer et al., 2010). As a result, low cloud response to sea ice variability may be undetectable to spaceborne LIDAR if it occurs below optically thick clouds.

Ship-based observations available during summer provide a totally independent data set that we use to corroborate spaceborne LIDAR observations. Ship-based visual cloud observations (Figure 5) confirm the result found using spaceborne LIDAR. During summer, there is no notable difference in low cloud cover over open water compared with sea ice. In the Western Hemisphere, locations of ship-based observations (Figure 5b) overlap well with the intermittent mask used for CALIPSO observations (Figure 4). Though we have no ship-based observations over most of the eastern hemisphere, we do not consider this to be a

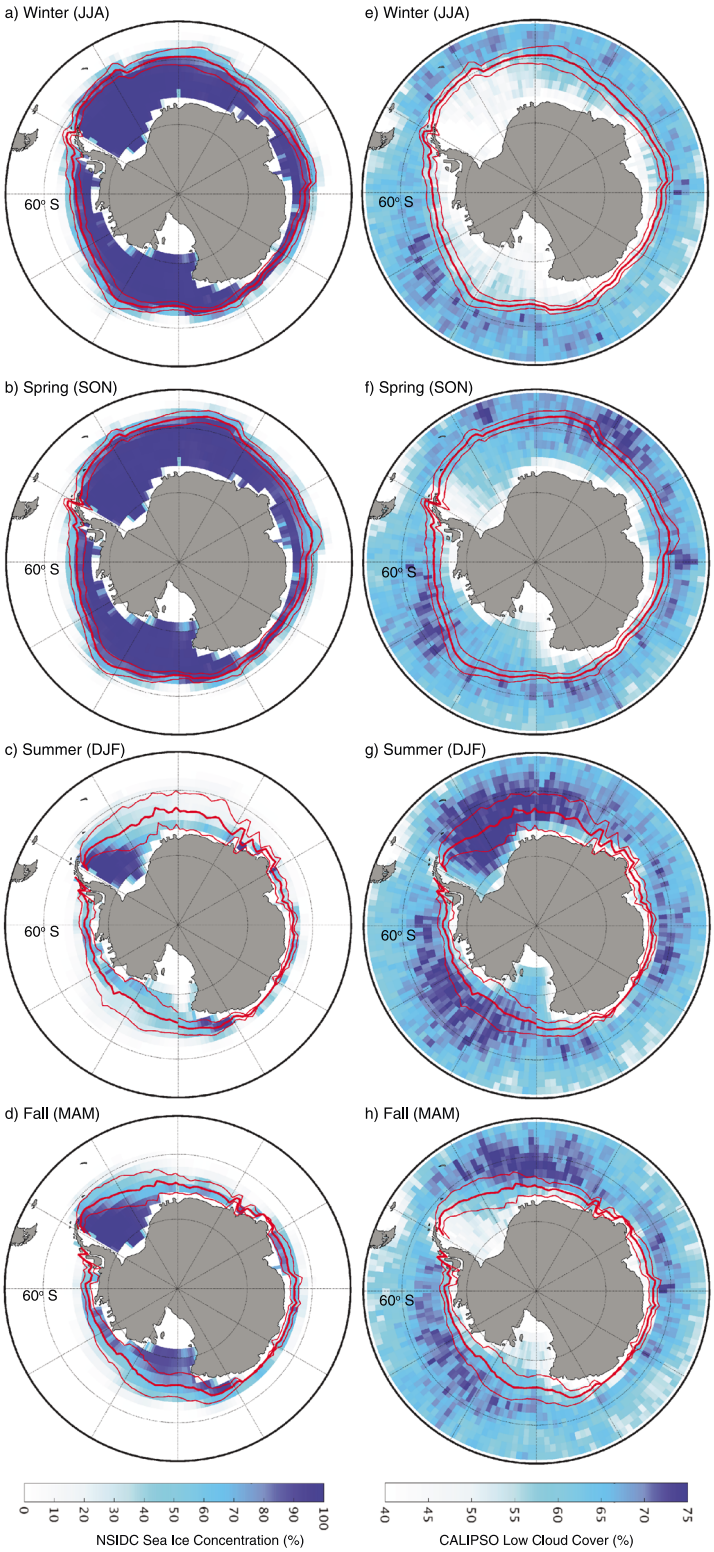


**Figure 2.** Seasonal Antarctic sea ice and low cloud cover. Mean NSIDC sea ice concentration (colored) (Peng et al., 2013) during winter (a), spring (b), summer (c), and fall (d). Mean CALIPSO GOCCP low cloud cover (colored) (Chepfer et al., 2010) during winter (e), spring (f), summer (g), and fall (h). Low cloud defined as cloud below 680 hPa. Bold red line shows mean seasonal position of the sea ice edge, thin red lines show ±1 standard deviation for the sea ice edge. Sea ice edge defined for each day and longitude as the furthest equatorward occurrence of sea ice concentration greater than or equal to 35% (Wall, Kohyama, et al., 2017). Data are from 2006 to 2015.

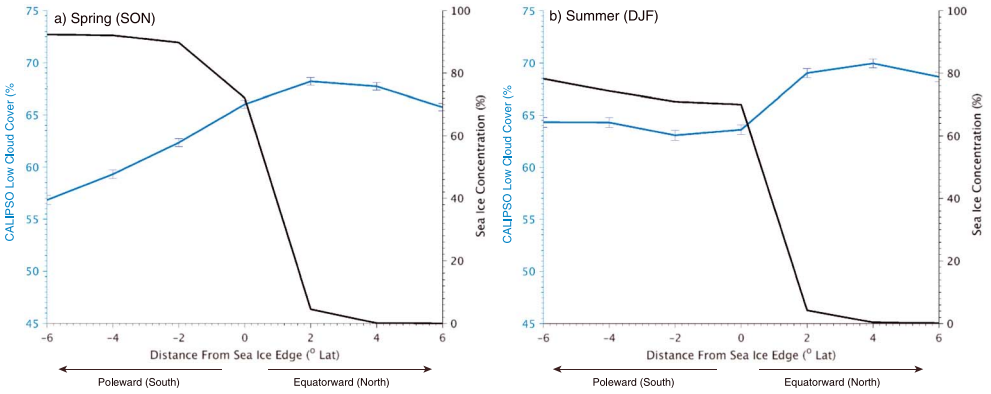


**Figure 3.** Spring and summer low cloud cover and sea ice concentration as a function of meridional distance from the sea ice edge. Mean CALIPSO low cloud cover (blue) and mean NSIDC sea ice concentration (black) versus meridional distance from the sea ice edge for spring (a) and summer (b). See the first method in section 2.2 for detailed methodology. Results shown are averages using daily data from 2006 to 2015. Error bars on low cloud cover show a 95% confidence interval using the *t* distribution.

serious limitation given that CALIPSO observations showed no hemispheric difference in cloud response (Figure 4).

### 3.4. Spring and Summer Cloud Opacity Response to Sea Ice Variability

Though the cloud cover response to sea ice variability is small in spring and near zero in summer, cloud opacity also matters. For example, cloud optical depth increases in response to sea ice loss could lessen the magnitude of top-of-atmosphere albedo decreases, or the top-of-atmosphere albedo could even

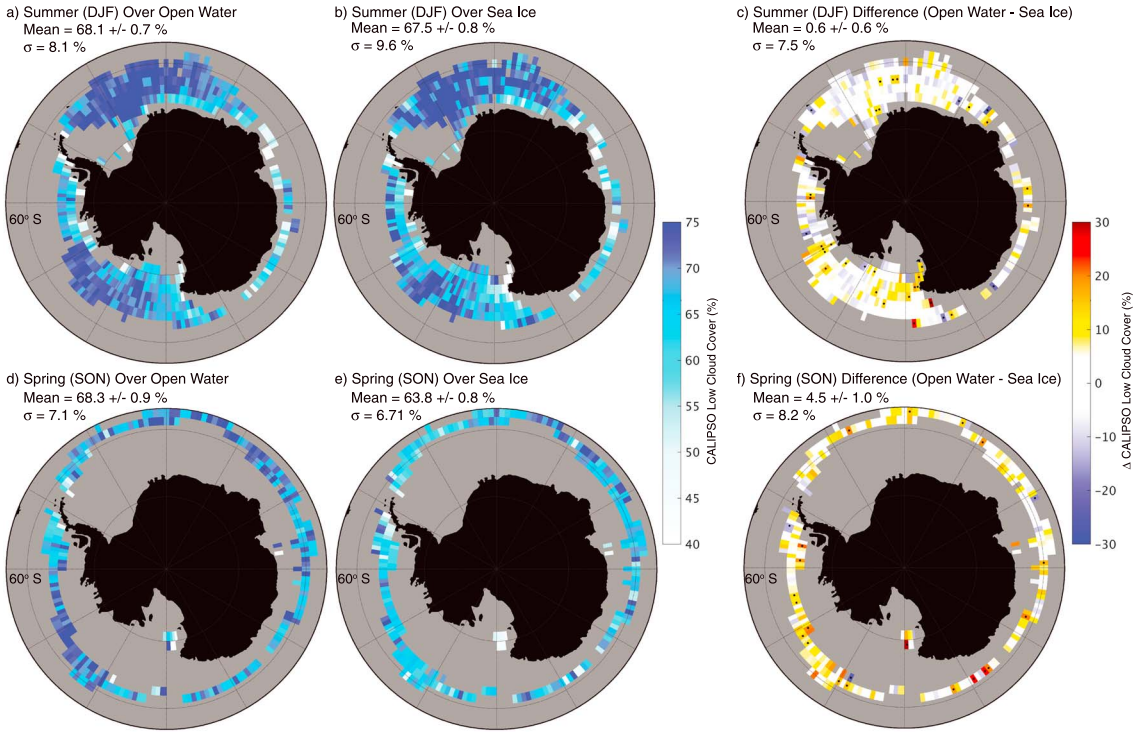


**Figure 4.** Low cloud cover within the intermittent mask. CALIPSO low cloud cover during summer over open water (sea ice concentration $< 15\%$) (a), over sea ice (sea ice concentration $> 80\%$) (b), and their difference (open water minus sea ice) (c). (d–f) As in (a)–(c) but for spring. Gray area in each panel shows ocean grid cells not included in the intermittent mask (section 2.2). The top left of each panel displays the mean (±95% confidence interval using *t* distribution) and standard deviation over the intermittent mask. Stippling in (c) and (f) show differences statistically significant at the 95% level using a Student's *t* test. Mean of daily data shown (2006–2015).

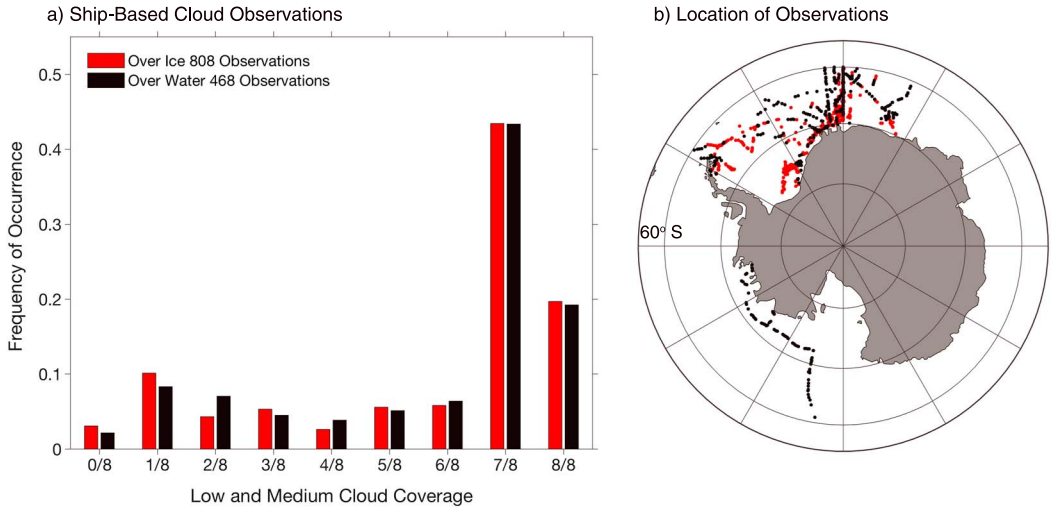


**Figure 5.** Ship-based cloud observations. (a) Histograms of summer low and medium cloud cover over sea ice (red) and over open water (black) created using visual sea ice and cloud observations (König-Langlo et al., 2006) from 13 research cruises (Table 1). (b) Locations of observations taken over sea ice (red) and over open water (black). Cloud cover and sea ice arrangement and concentration reported using standard World Meteorological Organization (WMO) reporting values (König-Langlo et al., 2006). A visual sea ice observation is defined as "open water" if sea ice is reported as "no ice in sight" or "sea ice present in concentration less than 3/10", while an observation is defined as "sea ice" if sea ice concentration is reported as "7/10 to 8/10" or "9/10 or more." Low and medium cloud cover is reported in eighths of cover.

increase (Fitzpatrick & Warren, 2007). Vertical profiles of relative humidity and temperature taken during Polarstern research cruises (Table 1) suggest increased cloud optical depth over open water. Relative humidity is higher over open water compared to sea ice in the lowest 2 km (Figure 6a). Additionally, temperature profiles over open water are warmer than those over sea ice (Figure 6b), which could suggest an increase in optical depth (see detailed discussion in section 4.2).

Consistent with ship-based profiles of relative humidity and temperature, CALIPSO observations also suggest an increase in optical depth over open water compared to sea ice. The fraction of opaque clouds (clouds that fully attenuate the LIDAR) is larger over open water compared to sea ice in both summer and spring (Figure 7). The increase in the opaque cloud fraction (defined as opaque cloud cover divided by total [opaque + thin] cloud cover) suggests that the overall optical depth of clouds and their shortwave radiative effect (Guzman et al., 2017) increase over open water compared with sea ice. The altitude of LIDAR attenuation in opaque clouds also changes over sea ice compared to open water. Near the surface, the altitude of full attenuation is higher over open water than it is over sea ice (Figure 8). When combined with relative humidity profiles (Figure 6) this higher altitude of attenuation is consistent with a thicker cloud layer over open water. In summary, changes in observed relative humidity and temperature (Figure 6), opaque cloud fraction (Figure 7), and the altitude of attenuation (Figure 8) all suggest that clouds are optically thicker over open water compared with sea ice.

### 3.5. Combined Impact of Sea Ice Variability and Cloud Response on Top-of-Atmosphere Albedo

We next assess the joint influence of sea ice variability and clouds on top-of-atmosphere albedo. The cloud response to sea ice variability is not large enough to compensate for the decrease in surface albedo from sea ice to open water. CERES observations show that all-sky top-of-atmosphere albedo, which is influenced by both clouds and the surface, is lower over open water than over sea ice within the intermittent mask during both spring and summer (Figure 9 and Table 2). As a result, in both spring and summer more shortwave radiation is absorbed over open water than over sea ice (Table 2). This is a significant advance over previous work where the sign of the absorbed shortwave radiation change in response to summer sea ice variability was uncertain (Fitzpatrick & Warren, 2007). Even though the difference in top-of-atmosphere albedo over open water compared to sea ice has a larger magnitude in spring than summer, the absorbed shortwave radiation increase is larger in summer compared to spring because solar insolation is larger during summer (Table 2).

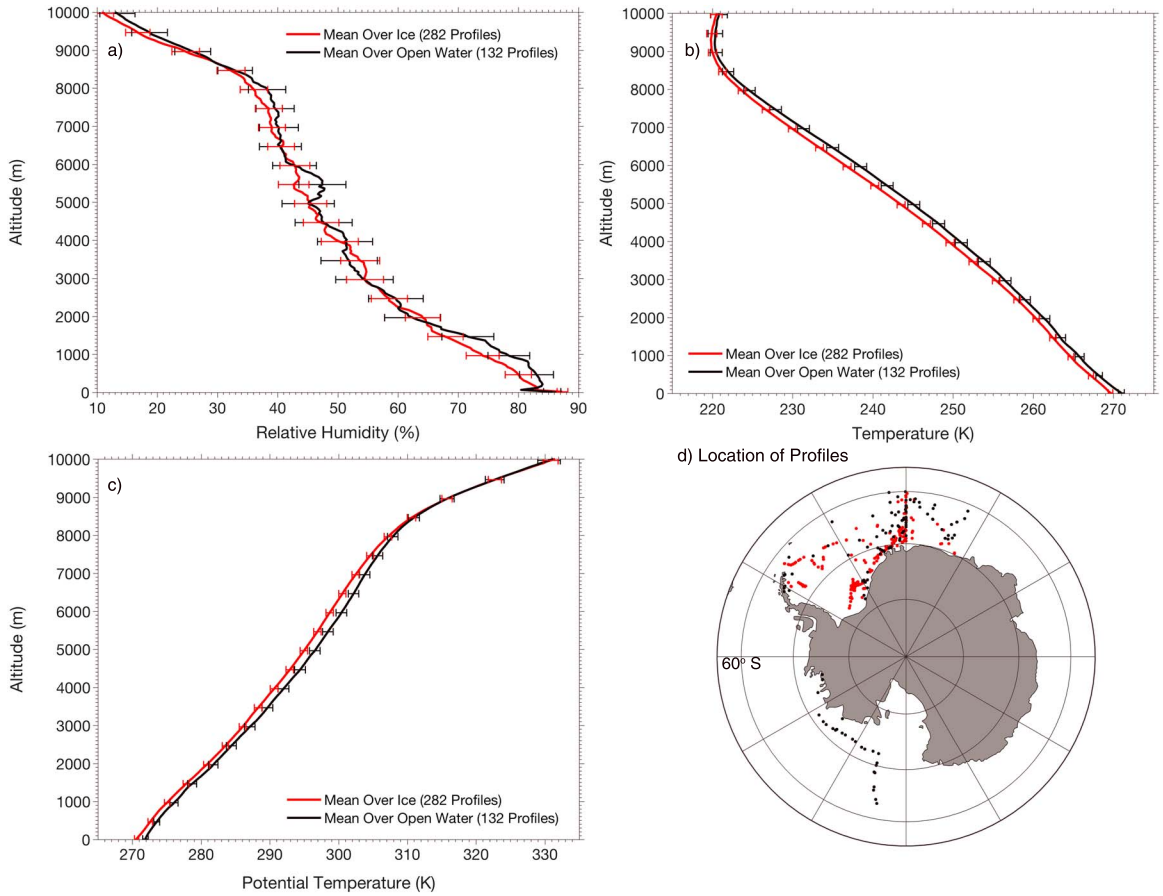


**Figure 6.** Ship-based meteorological profiles. Vertical profiles of relative humidity (a), temperature (b), and potential temperature (c). Locations of the soundings used to produce profiles (d). Over sea ice (red) and over open water (black). Error bars show 95% confidence interval (*t* distribution) every 500 m. Sea ice concentration assessed using visual sea ice observations as in Figure 5. Profiles taken with a vertical resolution of 50 m during summer between 2002 and 2016 (Table 1). Soundings are not always launched at times coinciding with sea ice observations, and here we only use profiles taken within 3 hr of a visual sea ice observation.

### 3.6. Insensitivity of Results to the Definitions of Sea Ice and Open Water

Our results are robust to differing definitions of sea and open water. To show this, we bin data within the intermittent mask by sea ice concentration to show how low cloud cover, opaque cloud fraction, and top-of-atmosphere albedo vary across the whole range of sea ice concentration (Figure 10). For low cloud cover and opaque cloud fraction any difference between open water and sea ice appears driven by the highest (95–100%) and lowest (0–5%) sea ice concentration bins. Top-of-atmosphere albedo increases with increasing sea ice concentration and is similar in spring and summer for sea ice concentration below 60%. Above 60% sea ice concentration, top-of-atmosphere albedo is higher in spring compared with summer, which likely is driven by differences in the optical properties of sea ice and the associated snow cover (Massom et al., 2001). We performed a similar analysis of top-of-atmosphere albedo using CERES SSF Level2 data (Loeb et al., 2005), which provides albedo data at the instantaneous footprint level. The resulting albedo values and patterns (not shown) are similar to Figure 10c, indicating that the gridding algorithm used for the SSF1deg product does not impact our results.

## 4. Discussion

### 4.1. Cloud and Albedo Response to Sea Ice Variability Revealed With Surface-Independent Observations

The most important result of this study is isolating the cloud and top-of-atmosphere albedo response to varying sea ice conditions in the Southern Ocean. We found no change (a small increase) in low cloud

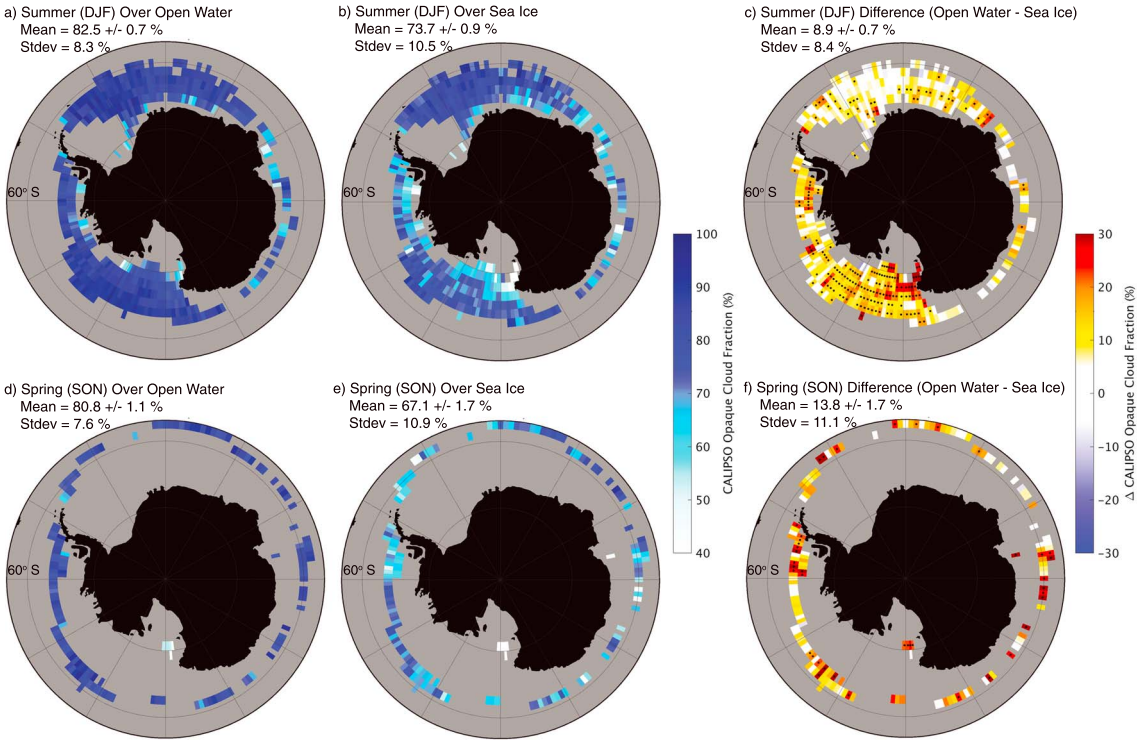


**Figure 7.** Opaque cloud fraction within the intermittent mask. As in Figure 4 but for opaque cloud fraction. Opaque cloud defined as clouds which fully attenuate the CALIPSO LIDAR (optical depth >3) (Guzman et al., 2017). Opaque cloud fraction defined as opaque cloud cover divided by total cloud cover. Mean of daily data shown (2007–2015).

cover during summer (spring) in response to decreased sea ice concentration (Figure 4). We also found more opaque cloud in summer and spring over open water compared to sea ice (Figure 7). Most importantly, even with the cloud response, top-of-atmosphere albedo is lower and more shortwave radiation is absorbed over open water than over sea ice (Figure 9). Because our results are based on observations that are independent of surface condition, they accurately reveal cloud changes occurring over open water compared to sea ice.

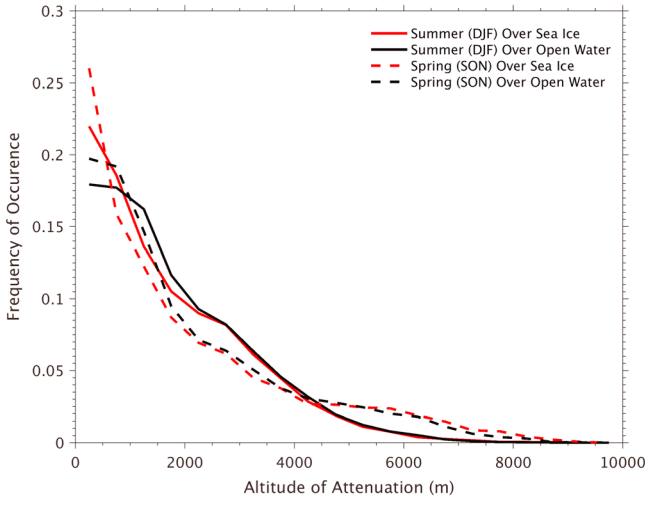


**Figure 8.** Probability density functions (PDF) of the altitude of CALIPSO LIDAR signal attenuation in opaque clouds over sea ice (red) and open water (black) during summer (solid) and spring (dashed). PDF created with daily CALIPSO-GOCCP data (Guzman et al., 2017) from 2007 to 2016 over the seasonal intermittent masks from Figure 7. PDF bin width is 500 meters.

### 4.2. Potential Mechanisms for Increasing Opaque Cloud Fraction

Surface-independent observations of temperature and cloud phase help constrain potential mechanisms underlying the observed cloud response to varying sea ice conditions. One potential mechanism leading to increased cloud opacity when sea ice retreats is an increase in air-sea coupling strength (Kay & Gettelman, 2009; Morrison et al., 2018; Wall, Kohyama, et al., 2017). Air-sea coupling contributes to low cloud formation and maintenance as moisture is transferred from the sea surface to the atmosphere to promote cloud formation (Klein & Hartmann, 1993). Interestingly, differences in air-sea coupling between open water and sea ice do not appear to drive the increase in summer opaque cloud fraction. We quantify the strength of air-sea coupling by assessing near-surface static stability the difference in potential temperature between 850 hPa and the surface. Potential temperature profiles (Figure 6c) indicate no significant difference in near-surface static stability over open water (5.3 K ± 0.7 K) compared with sea ice (5.6 K ± 0.4 K) during summer. Further, the difference

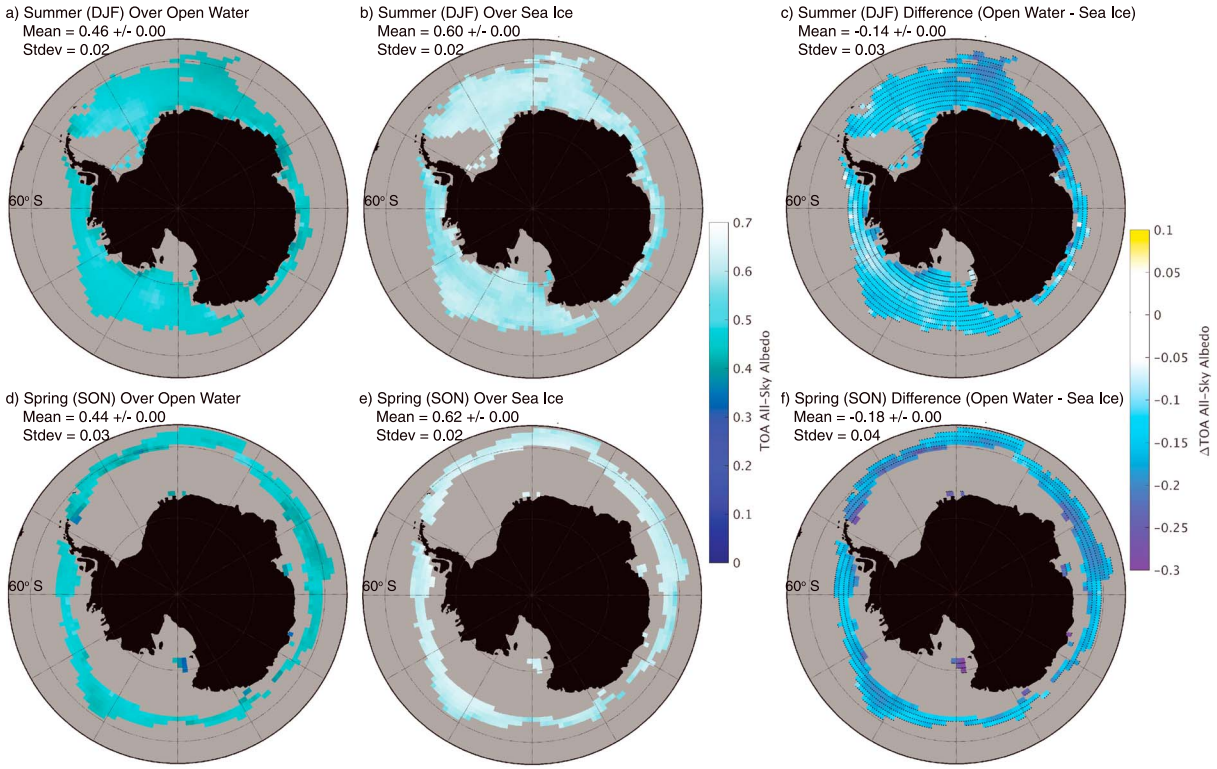


**Figure 9.** Top-of-atmosphere (TOA) all-sky albedo within the intermittent mask. As in Figure 4 but for CERES TOA all-sky albedo. Mean of daily data shown (2006–2015).

between surface air and sea temperature is small during summer (less than 1 K), which limits fluxes of moisture and heat from the sea to the atmosphere (Kay & Gettelman, 2009; Morrison et al., 2018).

A second potential mechanism leading to increased cloud opacity over open water as compared to over sea ice is an increase in temperature (Figure 6b). Increased temperatures lead to increased cloud opacity in the clouds prevalent over the Southern Ocean via two processes. In the first process, increased temperatures increase overall cloud water content as a result of an increased moist adiabatic lapse rate (e.g., Betts & Harshvardhan, 1987; Ceppi & Hartmann, 2016; Gordon & Klein, 2014; Somerville & Remer, 1984; Tselioudis et al., 1992). In the second process, increased temperatures result in more cloud liquid at the expense of cloud ice (e.g., Ceppi & Hartmann, 2016; Hu et al., 2010; McCoy et al., 2015, 2014). An increase in cloud liquid at the expense of ice increases optical depth even if overall water content is constant because cloud water droplets are much smaller than cloud ice crystals (Storelvmo et al., 2015). An increase in cloud liquid at the expense of ice also decreases precipitation efficiency, which can increase cloud liquid water content (Ceppi & Hartmann, 2016; Senior & Mitchell, 1993; Tsushima et al., 2006).

**Table 2**
*Summary of Main Findings*

| | Over open water | | Over sea ice | | Difference (open water − sea ice) | |
|---|---|---|---|---|---|---|
| Observation | Spring | Summer | Spring | Summer | Spring | Summer |
| CALIPSO low cloud cover | 68% | 68% | 64% | 68% | +4% | +0% |
| CALIPSO opaque cloud fraction | 81% | 83% | 67% | 74% | +14% | +9% |
| CERES top-of-atmosphere albedo | 0.44 | 0.46 | 0.62 | 0.60 | −0.18 | −0.14 |
| Estimated absorbed shortwave radiation | 164 W $m^{-2}$ | 238 W $m^{-2}$ | 112 W $m^{-2}$ | 176 W $m^{-2}$ | +53 W $m^{-2}$ | +62 W $m^{-2}$ |

*Note.* Spring and summer mean values of CALIPSO low cloud cover, CALIPSO opaque cloud fraction, and CERES top-of-atmosphere albedo over the region (shown in Figures 4, 7, and 9, respectively) where sea ice concentration varies. Estimated absorbed shortwave radiation calculated by multiplying one minus the mean top-of-atmosphere albedo by the mean solar insolation for each season over the appropriate region.

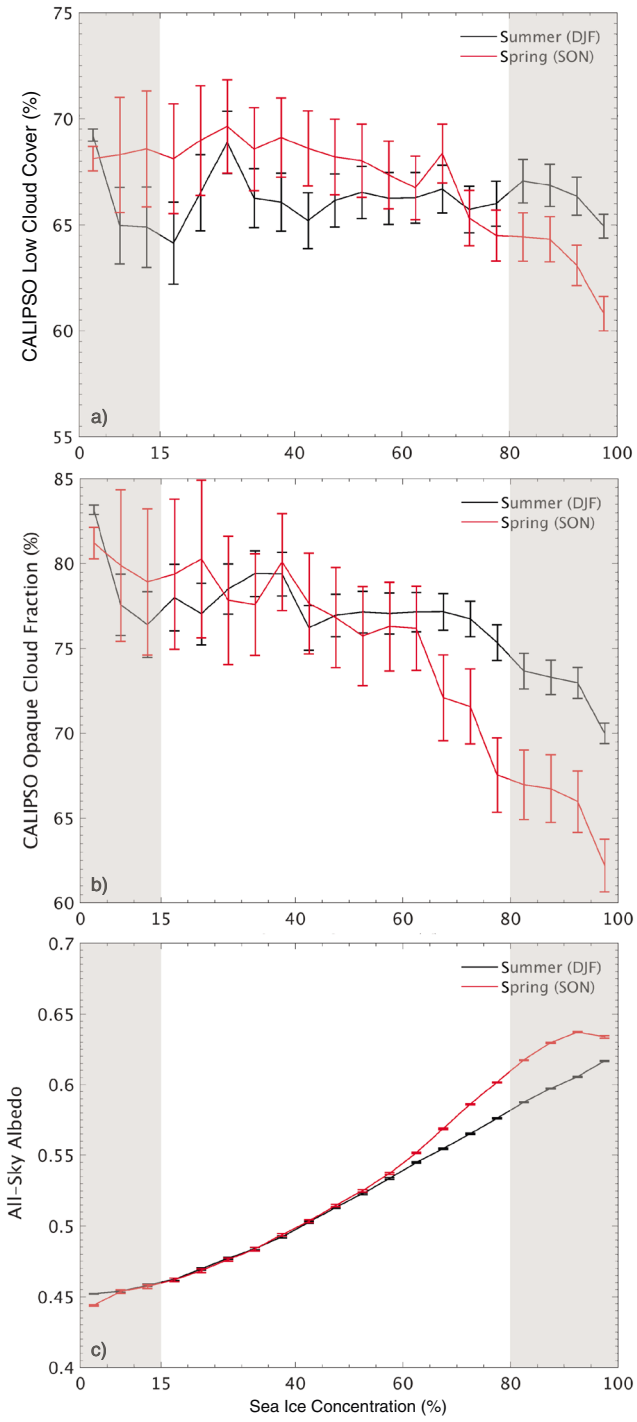


**Figure 10.** CALIPSO low cloud cover (a), CALIPSO opaque cloud fraction (b), and CERES top-of-atmosphere all-sky albedo (c) as a function of NSIDC sea ice concentration within the intermittent masks shown in Figures 4, 7, and 9, respectively, during summer (black) and spring (red). Data binned based on daily sea ice concentration (bin width 5%) and then averaged within each bin. Error bars show 95% confidence interval using a *t* distribution. Shaded areas show definitions of open water and sea ice used for intermittent masks. Data from 2006 to 2015 in (a) and (c) and (b) from 2007 to 2015.

CALIPSO cloud phase classifications support the second mechanism for cloud opacity increase by indicating a cloud phase shift from ice toward liquid. CALIPSO-GOCCP classifies cloud as liquid, ice, or undefined using the polarization of returns (Cesana & Chepfer, 2013). A classification of "undefined" most likely corresponds to mixed-phase clouds (Cesana et al., 2016). We use these classifications within the intermittent mask (as in Figure 4) to compare cloud phase over open water to sea ice. During summer, low liquid cloud cover is virtually unchanged over open water compared to sea ice while low ice cloud cover decreases by 1.5% and the undefined low cloud cover increases by 2.1%. During spring, low liquid cloud cover and undefined low cloud cover both increase by 2.5% over open water compared with sea ice while low ice cloud cover decreases by 0.6%. In both seasons, we find a decrease in low ice cloud cover coupled with an increase in mixed-phase and liquid cloud cover. CALIPSO cloud phase classifications suggest that increased temperatures (Figure 6) lead to increased opaque cloud fraction (Figure 7) through a shift in cloud phase from ice toward liquid.

### 4.3. Influence of Sea Ice on Southern Ocean Shortwave Cloud Radiative Feedbacks

We conclude our discussion by considering the implications of the diagnosed cloud response to sea ice variability on Southern Ocean shortwave cloud radiative feedbacks. Models robustly predict a negative shortwave cloud feedback due to an optical depth increase with warming over the Southern Ocean sea ice zone (Ceppi & Hartmann, 2016; Ceppi et al., 2016; Klein et al., 2009; McCoy et al., 2015; Mitchell et al., 1989; Terai et al., 2016; Zelinka et al., 2012). Our observational analysis indicates that sea ice does not directly impact this feedback. The same mechanism that drives the Southern Ocean negative shortwave feedback in models, increased temperatures leading to a shift in cloud phase from ice toward liquid (Ceppi & Hartmann, 2016), also causes the observed increase in cloud opacity we show over open water compared to sea ice. Therefore, sea ice will likely contribute to Southern Ocean shortwave cloud radiative feedbacks only to the extent that decreased sea ice concentration is accompanied by increased temperatures.

## 5. Summary and Conclusions

Spaceborne LIDAR observations are used to diagnose the spring and summer cloud response to Southern Ocean sea ice variability. Over the Southern Ocean region where surface condition varies between sea ice and open water, we find the following:

1. During spring, there is a small increase in low cloud cover over open water compared to sea ice. During summer, sea ice variability does not impact low cloud cover (Figure 4).
2. During both spring and summer, the fraction of optically thick clouds increases over open water compared to sea ice (Figure 7).
3. During both spring and summer, top-of-atmosphere albedo is lower and more shortwave radiation is absorbed over open water compared to sea ice (Figure 9).

Entirely independent of the spaceborne LIDAR observations, ship-based observations available during summer also show no cloud cover response to sea ice variability (Figure 5). Even when the cloud response to sea ice variability is included, top-of-atmosphere albedo is lower and more

shortwave radiation is absorbed over open water compared to sea ice. The results imply the cloud response to sea ice loss accompanying warming in the future will only partly mask the positive surface ice albedo feedback. When sea ice is lost during spring and summer, the Southern Ocean will absorb more shortwave radiation, which will accelerate warming.

**Acknowledgments**

CALIPSO-GOCCP data are available from the ClimServ center (http://climserv.ipsl.polytechnique.fr/cfmip-obs/). CERES SSF1deg data are available at https://ceres.larc.nasa.gov/order_data.php. NSIDC sea ice data are available at https://nsidc.org/data/g02202. Ship-based observations from Polarstern research cruises are available at https://www.pangaea.de/expeditions/cr.php/Polarstern. Code necessary to reproduce the results is available at sftp://wfrey@cheyenne.ucar.edu upon request from William Frey (william.frey@colorado.edu). This work was supported by startup funds awarded to Jennifer Kay by the University of Colorado Cooperative Institute for Research in the Environmental Sciences and NASA award NNX16AP18G. Rodrigo Guzman was supported by Centre National d'Etudes Spatiales (CNES). William Frey was supported by the Air Force Institute of Technology. The views expressed in this article are those of the authors and do not reflect the official policy or position of the United States Air Force, Department of Defense, or the U.S. Government.

## References

Armour, K. C., Marshall, J., Scott, J. R., Donohoe, A., & Newsom, E. R. (2016). Southern Ocean warming delayed by circumpolar upwelling and equatorward transport. *Nature Geoscience*, *9*(7), 549–554. https://doi.org/10.1038/NGEO2731

Barton, N. P., Klein, S. A., Boyle, J. S., & Zhang, Y. Y. (2012). Arctic synoptic regimes: Comparing domain-wide Arctic cloud observations with CAM4 and CAM5 during similar dynamics. *Journal of Geophysical Research*, *117*, D15205. https://doi.org/10.1029/2012JD017589

Betts, A. K., & Harshvardhan (1987). Thermodynamic constraint on the cloud liquid water feedback in climate models. *Journal of Geophysical Research*, *92*(D7), 8483–8485. https://doi.org/10.1029/JD092iD07p08483

Bromwich, D. H., & Fogt, R. L. (2004). Strong trends in the skill of the ERA-40 and NCEP-NCAR Reanalysis in the high and midlatitudes of the Southern Hemisphere, 1958–2001. *Journal of Climate*, *17*(23), 4603–4619. https://doi.org/10.1175/3241.1

Bromwich, D. H., Fogt, R. L., Hodges, K. I., & Walsh, J. E. (2007). A tropospheric assessment of the ERA-40, NCEP, and JRA-25 global reanalyses in the polar regions. *Journal of Geophysical Research*, *112*, D10111. https://doi.org/10.1029/2006JD007859

Bromwich, D. H., Nicolas, J. P., Hines, K. M., Kay, J. E., Key, E. L., Lazzara, M. A., et al. (2012). Tropospheric clouds in Antarctica. *Reviews of Geophysics*, *50*, RG1004. https://doi.org/10.1029/2011RG000363

Bromwich, D. H., Nicolas, J. P., & Monaghan, A. J. (2011). An assessment of precipitation changes over Antarctica and the Southern Ocean since 1989 in contemporary global reanalyses. *Journal of Climate*, *24*(16), 4189–4209. https://doi.org/10.1175/2011JCLI4074.1

Ceppi, P., & Hartmann, D. L. (2016). Mechanisms of the negative shortwave cloud feedback in middle to high latitudes. *Journal of Climate*, *29*(1), 139–157. https://doi.org/10.1175/JCLI-D-15-0327.1

Ceppi, P., McCoy, D. T., & Hartmann, D. L. (2016). Observational evidence for a negative shortwave cloud feedback in middle to high latitudes. *Geophysical Research Letters*, *43*, 1331–1339. https://doi.org/10.1002/2015GL067499

Cesana, G., & Chepfer, H. (2013). Evaluation of the cloud thermodynamic phase in a climate model using CALIPSO-GOCCP. *Journal of Geophysical Research: Atmospheres*, *118*, 7922–7937. https://doi.org/10.1002/jgrd.50376

Cesana, G., Chepfer, H., Winker, D., Getzewich, B., Cai, X., Jourdan, O., et al. (2016). Using in situ airborne measurements to evaluate three cloud phase products derived from CALIPSO. *Journal of Geophysical Research: Atmospheres*, *121*, 5788–5808. https://doi.org/10.1002/2015JD024334

Chepfer, H., Bony, S., Winker, D., Cesana, G., Dufresne, J. L., Minnis, P., et al. (2010). The GCM-Oriented CALIPSO Cloud Product (CALIPSO-GOCCP). *Journal of Geophysical Research*, *115*, D00H16. https://doi.org/10.1029/2009JD012251

Driemel, A., Loose, B., Grobe, H., Rainer, S., & König-Langlo, G. (2016). 30 years of upper air soundings on board of R/V *POLARSTERN*. *Earth System Science Data*, *8*(1), 213–220. https://doi.org/10.5194/essd-8-213-2016

Eastman, R., & Warren, S. G. (2010). Interannual variations of Arctic cloud types in relation to sea ice. *Journal of Climate*, *23*(15), 4216–4232. https://doi.org/10.1175/2010JCLI3492.1

Fitzpatrick, M. F., & Warren, S. G. (2007). The relative importance of clouds and sea ice for the solar energy budget of the Southern Ocean. *Journal of Climate*, *20*(6), 941–954. https://doi.org/10.1175/JCLI4040.1

Frey, W. R., & Kay, J. E. (2018). The influence of extratropical cloud phase and amount feedbacks on climate sensitivity. *Climate Dynamics*, *50*(7-8), 3097–3116. https://doi.org/10.1007/s00382-017-3796-5

Frey, W. R., Maroon, E. A., Pendergrass, A. G., & Kay, J. E. (2017). Do Southern Ocean cloud feedbacks matter for 21st century warming? *Geophysical Research Letters*, *44*, 12,447–12,456. https://doi.org/10.1002/2017GL076339

Gordon, N. D., & Klein, S. A. (2014). Low-cloud optical depth feedback in climate models. *Journal of Geophysical Research: Atmospheres*, *119*, 6052–6065. https://doi.org/10.1002/2013JD021052

Guzman, R., Chepfer, H., Noel, V., Vaillant de Guelis, T., Kay, J. E., Raberanto, P., et al. (2017). Direct atmosphere opacity observations from CALIPSO provide new constraints on cloud-radiation interactions. *Journal of Geophysical Research: Atmospheres*, *122*, 1066–1085. https://doi.org/10.1002/2016JD025946

Hartmann, D. L., & Ceppi, P. (2014). Trends in the CERES dataset, 2000–13: The effects of sea ice and jet shifts and comparison to climate models. *Journal of Climate*, *27*(6), 2444–2456. https://doi.org/10.1175/JCLI-D-13-00411.1

Hines, K. M., Grumbine, R. W., Bromwich, D. H., & Cullather, R. I. (1999). Surface energy balance of the NCEP MRF and NCEP-NCAR Reanalysis in Antarctic latitudes during FROST. *Journal of Climate*, *14*(6), 851–866. https://doi.org/10.1175/1520-0434(1999)014%3C0851:SEBOTN%3E2.0.CO;2

Hoskins, B. J., & Hodges, K. I. (2005). A new perspective on Southern Hemisphere storm tracks. *Journal of Climate*, *18*(20), 4108–4129. https://doi.org/10.1175/JCLI3570.1

Hu, Y., Rodier, S., Xu, K., Sun, W., Huang, J., Lin, B., et al. (2010). Occurrence, liquid water content, and fraction of supercooled water clouds from combined CALIOP/IIR/MODIS measurements. *Journal of Geophysical Research*, *115*, D00H34. https://doi.org/10.1029/2009JD012384

Jones, R. W., Renfrew, I. A., Orr, A., Webber, B. G. M., Holland, D. M., & Lazzara, M. A. (2016). Evaluation of four global reanalysis products using in situ observations in the Amundsen Sea Embayment, Antarctica. *Journal of Geophysical Research: Atmospheres*, *121*, 6240–6257. https://doi.org/10.1002/2015JD024680

Kay, J. E., & Gettelman, A. (2009). Cloud influence on and response to seasonal Arctic Sea ice loss. *Journal of Geophysical Research*, *114*, D18204. https://doi.org/10.1029/2009JD011773

Kay, J. E., & L'Ecuyer, T. (2013). Observational constraints on Arctic Ocean clouds and radiative fluxes during the early 21st century. *Journal of Geophysical Research: Atmospheres*, *118*, 7219–7236. https://doi.org/10.1002/jgrd.50489

Kay, J. E., L'Ecuyer, T., Chepfer, H., Loeb, N., Morrison, A., & Cesana, G. (2016). Recent advances in Arctic cloud and climate research. *Current Climate Change Reports*, *2*(4), 159–169. https://doi.org/10.1007/s40641-016-0051-9

Klein, S. A., & Hartmann, D. L. (1993). The seasonal cycle of low stratiform clouds. *Journal of Climate*, *6*(8), 1587–1606. https://doi.org/10.1175/1520-0442(1993)006%3C1587:TSCOLS%3E2.0.CO;2

Klein, S. A., McCoy, R. B., Morrison, H., Ackerman, A. S., Avramov, A., Boer, G., et al. (2009). Intercomparison of model simulations of mixed-phase clouds observed during the ARM mixed-phase Arctic cloud experiment. I: Single-layer cloud. *Quarterly Journal of the Royal Meteorological Society*, *135*(641), 979–1002. https://doi.org/10.1002/qj.416

König-Langlo, G., Loose, B., & Bräuer, B. (2006). 25 years of Polarstern meteorology (1982–2006). *WDC-MARE Reports*, *4*, 1–137. https://doi.org/10.2312/wdc-mare.2006.4

Konsta, D., Dufresne, J.-L., Chepfer, H., Idelkadi, A., & Cesana, G. (2016). Use of A-train satellite observations (CALIPSO-PARASOL) to evaluate tropical cloud properties in the LMDZ5 GCM. *Climate Dynamics*, *47*(3-4), 1263–1284. https://doi.org/10.1007/s00382-015-2900-y

Kopp, G., Lawrence, G., & Rottman, G. (2005). The Total Irradiance Monitor (TIM): Science results. In G. Rottman, T. Woods, & V. George (Eds.), *The Solar Radiation and Climate Experiment (SORCE)* (pp. 129–139). New York: Springer. https://doi.org/10.1007/0-387-37625-9_8

Leahy, L. V., Wood, R., Charlson, R. J., Hostetler, C. A., Rogers, R. R., Vaughan, M. A., & Winker, D. M. (2012). On the nature and extent of optically thin marine low clouds. *Journal of Geophysical Research*, *117*, D22201. https://doi.org/10.1029/2012JD017929

Liu, Y., Ackerman, S. A., Maddux, B. C., Key, J. R., & Frey, R. A. (2010). Errors in cloud detection over the Arctic using a satellite imager and implications for observing feedback mechanisms. *Journal of Climate*, *23*(7), 1894–1907. https://doi.org/10.1175/2009JCLI3386.1

Loeb, N. G., Kato, S., Loukachine, K., & Manalo-Smith, N. (2005). Angular distribution models for top-of-atmosphere radiative flux estimation from the clouds and the Earth's radiant energy system instrument on the *Terra* satellite. Part I: Methodology. *Journal of Atmospheric and Oceanic Technology*, *22*(4), 338–351. https://doi.org/10.1175/JTECH1712.1

Marshall, G. J. (2002). Trends in Antarctic geopotential height and temperature: A comparison between radiosonde and NCEP-NCAR reanalysis data. *Journal of Climate*, *15*(6), 659–674. https://doi.org/10.1175/1520-0442(2002)015%3C0659:TIAGHA%3E2.0.CO;2

Marshall, J., & Speer, K. (2012). Closure of the meridional overturning circulation through Southern Ocean upwelling. *Nature Geoscience*, *5*(3), 171–180. https://doi.org/10.1038/NGEO1391

Massom, R. A. A., Eicken, H., Haas, C., Jeffries, M. O., Drinkwater, M. R., Sturm, M., & Worby, A. P. (2001). Snow on Antarctic Sea ice. *Reviews of Geophysics*, *39*(3), 413–445. https://doi.org/10.1029/2000RG000085

McCoy, D. T., Hartmann, D. L., & Grosvenor, D. P. (2014). Observed Southern Ocean cloud properties and shortwave reflection. Part I: Calculation of SW flux from observed cloud properties. *Journal of Climate*, *27*(23), 8836–8857. https://doi.org/10.1175/JCLI-D-14-00287.1

McCoy, D. T., Hartmann, D. L., Zelinka, M. D., Ceppi, P., & Grosvenor, D. P. (2015). Mixed-phase cloud physics and Southern Ocean cloud feedback in climate models. *Journal of Geophysical Research: Atmospheres*, *120*, 9539–9554. https://doi.org/10.1002/2015JD023603

Meier, W., Fetterer, F., Savoie, M., Mallory, S., Duerr, R., & Stroeve, J. (2017). *NOAA/NSIDC climate data record of passive microwave sea ice concentration, version 3. Boulder, Colorado USA*. NSIDC: National Snow and Ice Data Center. https://doi.org/10.7265/N59P2ZTG

Mitchell, J. F. B., Senior, C. A., & Ingram, W. J. (1989). $CO_2$ and climate: A missing feedback? *Nature*, *341*(6238), 132–134. https://doi.org/10.1038/341132a0

Morrison, A. L., Kay, J. E., Chepfer, H., Guzman, R., & Yettella, V. (2018). Isolating the liquid cloud response to recent Arctic Sea ice variability using spaceborne lidar observations. *Journal of Geophysical Research: Atmospheres*, *123*, 473–490. https://doi.org/10.1002/2017JD027248

Nicolas, J. P., & Bromwich, D. H. (2011). Precipitation changes in high southern latitudes from global reanalyses: A cautionary tale. *Surveys in Geophysics*, *32*(4-5), 475–494. https://doi.org/10.1007/s10712-011-9114-6

Palm, S. P., Strey, S. T., Spinhirne, J., & Markus, T. (2010). Influence of Arctic sea ice extent on polar cloud fraction and vertical structure and implications for regional climate. *Journal of Geophysical Research*, *115*, D21209. https://doi.org/10.1029/2010JD013900

Peng, G., Meier, W. N., Scott, D. J., & Savoie, M. H. (2013). A long-term and reproducible passive microwave sea ice concentration data record for climate studies and monitoring. *Earth System Science Data*, *5*(2), 311–318. https://doi.org/10.5194/essd-5-311-2013

Qu, X., & Hall, A. (2005). Surface contribution to planetary albedo variability in cryosphere regions. *Journal of Climate*, *18*(24), 5239–5252. https://doi.org/10.1175/JCLI3555.1

Schweiger, A. J., Lindsay, R. W., Vavrus, S., & Francis, J. A. (2008). Relationships between Arctic sea ice and clouds during autumn. *Journal of Climate*, *21*(18), 4799–4810. https://doi.org/10.1175/2008JCLI2156.1

Senior, C. A., & Mitchell, J. F. B. (1993). Carbon dioxide and climate: The impact of cloud parameterization. *Journal of Climate*, *6*(3), 393–418. https://doi.org/10.1175/1520-0442(1993)006%3C0393:CDACTI%3E2.0.CO;2

Serreze, M. C., Barrett, A. P., Stroeve, J. C., Kindig, D. N., & Holland, M. M. (2009). The emergence of surface-based Arctic amplification. *The Cryosphere*, *3*(1), 11–19. https://doi.org/10.5194/tc-3-11-2009

Simmons, I. (2015). Comparing and contrasting the behaviour of Arctic and Antarctic sea ice over the 35 year period 1979–2013. *Annals of Glaciology*, *56*(69), 18–28. https://doi.org/10.3189/2015AoG69A909

Somerville, R. C. J., & Remer, L. (1984). Cloud optical thickness feedbacks in the $CO_2$ climate problem. *Journal of Geophysical Research*, *89*(D6), 9668–9672. https://doi.org/10.1029/JD089iD06p09668

Stammerjohn, S., Massom, R., Rind, D., & Martinson, D. (2012). Regions of rapid sea ice change: An inter-hemispheric seasonal comparison. *Geophysical Research Letters*, *39*, L06501. https://doi.org/10.1029/2012GL050874

Storelvmo, T., Tan, I., & Korolev, A. V. (2015). Cloud phase changes induced by $CO_2$ warming—A powerful yet poorly constrained cloud-climate feedback. *Current Climate Change Reports*, *1*(4), 288–296. https://doi.org/10.1007/s40641-015-0026-2

Tan, I., Storelvmo, T., & Zelinka, M. D. (2016). Observational constraints on mixed-phase clouds imply higher climate sensitivity. *Science*, *352*(6282), 224–227. https://doi.org/10.1126/science.aad5300

Taylor, P. C., Kato, S., Xu, K.-M., & Cai, M. (2015). Covariance between Arctic Sea ice and clouds within atmospheric state regimes at the satellite footprint level. *Journal of Geophysical Research: Atmospheres*, *120*, 12,656–12,678. https://doi.org/10.1002/2015JD023520

Terai, C. R., Klein, S. A., & Zelinka, M. D. (2016). Constraining the low-cloud optical depth feedback at middle and high latitudes using satellite observations. *Journal of Geophysical Research: Atmospheres*, *121*, 9696–9716. https://doi.org/10.1002/2016JD025233

Town, M. S., Walden, V. P., & Warren, S. G. (2007). Cloud cover over the South Pole from visual observations, satellite retrievals, and surface-based infrared radiation measurements. *Journal of Climate*, *20*(3), 544–559. https://doi.org/10.1175/JCLI4005.1

Tselioudis, G., Rossow, W. B., & Rind, D. (1992). Global patterns of cloud optical thickness variation with temperature. *Journal of Climate*, *5*(12), 1484–1495. https://doi.org/10.1175/1520-0442(1992)005%3C1484:GPOCOT%3E2.0.CO;2

Tsushima, Y., Emori, S., Ogura, T., Kimoto, M., Webb, M. J., Williams, K. D., et al. (2006). Importance of the mixed-phase cloud distribution in the control climate for assessing the response of clouds to carbon dioxide increase: A multi-model study. *Climate Dynamics*, *27*(2-3), 113–126. https://doi.org/10.1007/s00382-006-0127-7

Wall, C. J., Hartmann, D. L., & Ma, P.-L. (2017). Instantaneous linkages between clouds and large-scale meteorology over the Southern Ocean in observations and a climate model. *Journal of Climate*, *30*(23), 9455–9474. https://doi.org/10.1175/JCLI-D-17-0156.1

Wall, C. J., Kohyama, T., & Hartmann, D. L. (2017). Low-cloud, boundary layer, and sea ice interactions over the Southern Ocean during winter. *Journal of Climate*, *30*(13), 4857–4871. https://doi.org/10.1175/JCLI-D-16-0483.1

Warren, S. G., Eastman, R. M., & Hahn, C. J. (2007). A survey of changes in cloud cover and cloud types over land from surface observations, 1971–96. *Journal of Climate*, *20*(4), 717–738. https://doi.org/10.1175/JCLI4031.1

Winker, D. M., Hunt, W. H., & McGill, M. J. (2007). Initial performance assessment of CALIOP. *Geophysical Research Letters*, *34*, L19803. https://doi.org/10.1029/2007GL030135

Zelinka, M. D., Klein, S. A., & Hartmann, D. L. (2012). Computing and partitioning cloud feedbacks using cloud property histograms. Part II: Attribution to changes in cloud amount, altitude, and optical depth. *Journal of Climate*, *25*(11), 3736–3754. https://doi.org/10.1175/JCLI-D-11-00249.1

Zelinka, M. D., Klein, S. A., & Hartmann, D. L. (2012). Computing and partitioning cloud feedbacks using cloud property histograms. Part I: Cloud radiative kernels. *Journal of Climate*, *25*(11), 3715–3735. https://doi.org/10.1175/JCLI-D-11-00248.1